www.czasopisma.pan.pl PAN POLSKA AKADEMIA NAUK www.journals.pan.pl

Arch. Metall. Mater. **70** (2025), 4, 1913-1926

DOI: https://doi.org/10.24425/amm.2025.156278

ENHUI WU[1,2,3], PENG LIU[1,2,3,4*], JUN LI[1,2,3], LILIN MU[1], JING HOU[1,2,3], ZHONG XV[1,2,3], BO ZHANG[4], JUN DOU[4], SHUZHONG CHEN[4]

# EFFECT AND MECHANISMS OF OXIDATIVE ROASTING MINERAL PHASE RECONSTRUCTION WITH MgO AND LEACHING IN DIRECT EXTRACTION OF V FROM TITANOMAGNETITE CONCENTRATE

The technology for directly extracting vanadium from titanomagnetite concentrate boasts low energy consumption, a streamlined process, and a high recovery rate, thereby holding immense significance for advancements in various fields, including Ti-Al-V alloys, vanadium catalysts, and all-vanadium redox flow batteries. Research findings on the oxidative roasting and V leaching process of magnesium compounds within this concentrate revealed optimal conditions for hydrochloric acid/sulfuric acid leaching: an acid concentration of 1.5 mol/L, a leaching temperature of 55°C, and a liquid-to-solid ratio of 8, when the leaching duration was set at 2 hours. Under these parameters, the introduction of 3 wt.% MgO, $MgCO_3$, and $Mg(OH)_2$ to titanomagnetite concentrate oxidative roasting led to ore phase reconstruction, subsequently enhancing the V leaching efficiency by 5.19%, 2.92%, and 4.21%, respectively. The highest V leaching efficiency of 64.4% was achieved with the addition of MgO for mineral phase reconstruction. This enhancement was attributed to the local shrinkage and pore-forming mechanisms within the lattice structure facilitated by MgO. Furthermore, calculations on the variations in the concentrations of 12 V-related ions in the V-$H_2O$ system across different pH values indicated that V predominantly existed in the form of $VO_2^+$ in the leachate. The H-free large ion in the V-$H_2O$ system, $V_{10}O_{28}^{6-}$, comprised 31.4% V at pH 6 and exhibited a tendency towards precipitation. The stable generation of this ion occurred within pH 5-6.3, which could be deemed as the optimal pH range for V precipitation in the V-$H_2O$ system.

*Keywords:* Direct extraction of V; mineral phase reconstruction; leaching; mechanisms; V-$H_2O$ system

## 1. Introduction

Vanadium is not found as a standalone mineral [1]. Instead, 98% of its reserves are embedded within titanomagnetite, while the remaining percentage exists in various forms of multi-valent oxides, often in association with phosphate rocks, uranium-bearing sandstones, siltstone ores, as well as shale vanadium ores that include stone coal and coal gangue [2-4]. Considered a crucial rare metal element, vanadium finds extensive utilization across diverse industries such as steel production, high-end metal materials, chemicals, energy storage solutions, pigments, nanomaterials, and medical materials [1,5-7]. Notably, the steel sector accounts for over 85% of vanadium consumption [8,9]. Vanadium-enhanced steel boasts exceptional strength, toughness, and wear resistance, rendering it indispensable for applications in machinery, automotive, shipbuilding, railways, aviation, bridges, electronic technology, and defense industries. Furthermore, vanadium plays a pivotal role in the production of titanium-aluminum-vanadium alloys, catalysts, and all-vanadium redox flow batteries [10-15]. Specifically, the emergence of all-vanadium redox flow batteries as a novel application of vanadium is poised to stimulate significant growth in the vanadium market, driven by the expanding energy storage industry [13-15].

TABLE 1

Sources of vanadium production in 2020 and 2021

| Sources | | Direct extraction of V | Vanadium rich steel slag | Spent catalyst | Stone coal |
|---|---|---|---|---|---|
| 2020 | Global | 7.21% | 74.8% | 11.4% | 6.59% |
| | China | 0.29% | 86.9% | 2.1% | 10.7% |
| 2021 | Global | 7.74% | 76% | 11% | 5.26% |
| | China | 0.9% | 88.7% | 2.6% | 7.8% |

According to TABLE 1 [8,9], approximately 84% of global vanadium production originates from titanomagnetite. Direct extraction from titanomagnetite concentrate accounts

[1] PANZHIHUA UNIVERSITY, PANZHIHUA 617000, CHINA
[2] SICHUAN PROVINCIAL KEY LABORATORY OF VANADIUM-TITANIUM KEY STRATEGIC MATERIALS, PANZHIHUA 617000, CHINA
[3] SICHUAN PROVINCE ENGINEERING TECHNOLOGY RESEARCH CENTER OF VANADIUM AND TITANIUM MATERIALS, PANZHIHUA 617000, CHINA
[4] LB SICHUAN MINING AND METALLURGY CO., LTD, PANZHIHUA 617000, CHINA

* Corresponding author: tbagmo@126.com

for about 7.5% (primarily in South Africa and Brazil), while extraction from vanadium-rich steel slag makes up about 76% (primarily in China and Russia). Additionally, secondary resource utilization and stone coal (unique to China) contribute approximately 17.5% of the total production. It is evident that vanadium-rich steel slag, derived primarily from titanomagnetite, is the primary source of vanadium production. However, it is deeply intertwined with the blast furnace ironmaking route and converter vanadium extraction, characterized by high equipment thresholds and long processes. Consequently, vanadium production capacity is closely associated with steel output, $CO_2$ emissions. While this has minimal impact on vanadium's application in the steel industry, it significantly affects its development in emerging energy storage fields like all-vanadium redox flow batteries. Due to the deep binding between vanadium production capacity from vanadium-rich steel slag and blast furnace processes, which rely heavily on blast furnace process, the rapid market expansion of all-vanadium redox flow batteries would undoubtedly generate significant market demand. As a result, vanadium production would gradually face constraints imposed by steel production capacity and $CO_2$ emissions, hindering the flexible development of emerging energy storage industries such as all-vanadium redox flow batteries. Moreover, the reliance on a single vanadium production source like vanadium-rich steel slag, which heavily depends on blast furnace process, is unfavorable for the recycling and utilization of titanium resources [16,17]. Therefore, to adjust the source structure of vanadium production, better promote the development of the all-vanadium redox flow battery industry, and accelerate the comprehensive utilization of valuable metals in titanomagnetite concentrate, it is necessary to research and optimize direct vanadium extraction techniques from this ore.

Direct vanadium extraction technology has been increasingly garnering attention due to its low energy consumption, shorter process flow, and high recovery rates [18]. This method typically employs titanomagnetite concentrate as the feedstock for pellet preparation. Under high-temperature conditions, these pellets undergo mineral phase reconstruction. Following this, the material is crushed and ball-milled before undergoing acid leaching to extract the vanadium. The resulting filter residue, after drying, can serve as a high-quality iron concentrate product. Meanwhile, the filtrate is further processed using ammonia to extract the vanadium. Upon drying and calcination, $V_2O_5$ is obtained as the final product. Additionally, other valuable metals such as Al, and Mg can be selectively separated at different pH ranges during the process. In essence, the utilization of titanomagnetite concentrate in direct vanadium extraction technology offers a viable and efficient means of obtaining high-quality iron concentrate and $V_2O_5$, while also allowing for the separation of other valuable metals.

Research on the direct extraction of vanadium from titanium magnetite concentrate primarily focuses on four aspects: mineral phase reconstruction, leaching, vanadium precipitation, and calcination. The addition of sodium salts, such as $Na_2CO_3$, $Na_2SO_3$, or NaCl, to titanium magnetite concentrate during roasting can effectively alter the mineral structure and form sodium metavanadate, enabling direct water leaching. However, this process consumes a significant amount of sodium salts and generates water-insoluble double salts like sodium iron titanate and sodium aluminosilicate, leading to high residual sodium ions in the leaching residue that cannot be recovered. These residues can cause blockages in blast furnaces and corrode the furnace lining. Furthermore, when sodium sulfate or sodium chloride is used as a sodium salt additive, harmful gases such as sulfur dioxide and chlorine are released during roasting, increasing treatment costs and negatively impacting environmental quality [19-24].The addition of calcium salts, such as calcium carbonate or calcium oxide, to titanium magnetite concentrate during the roasting process can effectively alter the mineral structure and facilitate the formation of calcium vanadate, which is directly leachable by acid. While this method circumvents the high residual sodium ion issue associated with sodium salt roasting, it leads to the formation of calcium ferrite, which is soluble in acid, thereby increasing the iron loss rate. Furthermore, if dilute sulfuric acid is used for leaching, it results in a certain degree of sulfur ion residue, posing environmental pollution concerns [25-30].The addition of magnesium compounds, such as MgO, $MgCO_3$, or $Mg(OH)_2$, to titanium magnetite concentrate, followed by oxidative roasting, can effectively alter the mineral structure and enhance vanadium leaching efficiency. Importantly, compared to traditional sodium-based and calcium-based roasting processes, magnesium compounds can be recovered during vanadium precipitation, avoiding sodium and sulfur ion residues, reducing the generation of solid waste and wastewater, and promoting environmental sustainability. This advancement holds significant importance for the progress of direct vanadium extraction technology [31].

This study used titanomagnetite concentrate as the raw material to investigate the process of oxide roasting and mineral phase reconstruction with the addition of magnesium compounds, as well as its impact on acid leaching effectiveness. The aim was to reveal the mechanism of mineral phase reconstruction with magnesium compounds and provide a theoretical foundation for the advancement of direct vanadium extraction technology from titanomagnetite concentrate.

## 2. Materials and methods

### 2.1. Materials

The chemical composition of the titanomagnetite concentrate sample, as presented in TABLE 2 (with $Fe_3O_4$ and $V_2O_5$ mass fractions as calculated values), revealed that iron oxides and titanium oxides constituted over 80% of its content. These oxides primarily existed in the form of $Fe_3O_4$-like substances and $FeTiO_3$ (as shown in Fig. 1a), representing the major intergrown phases within the titanomagnetite concentrate. The $Fe_3O_4$-like substances, characterized by a stable inverse spinel structure and a dense face-centered cubic atomic arrangement, enclosed most of the low-valent V elements (depicted in Fig. 1b) through isomorphous substitution (replacing Fe atoms within the $Fe_3O_4$

lattice), resulting in the inability of XPS characterization to detect significant V2p 3/2 characteristic peaks.

This enclosure made it challenging for these V elements to contact with acid solutions during the leaching process. The microstructure is shown in Fig. 1c-f, where Fig. 1d is a partial enlargement of Fig. 1c, and Fig. 1e/f are the corresponding mapping results of Fig. 1d area; Fig. 1g indicated that the surface of the lattice structure was composed of divalent iron. Titanomagnetite concentrates with iron oxide crystal structure particles would try to encapsulate trivalent iron as much as possible inside, while exposing divalent iron on the surface. This was because trivalent iron tended to bond with more oxygen atoms, and encapsulating it inside could stabilize its bonding electrons and reduce system energy; Although the presence of divalent iron atoms on the surface of particles could result in non-bonding of valence electrons, compared to exposing trivalent iron atoms

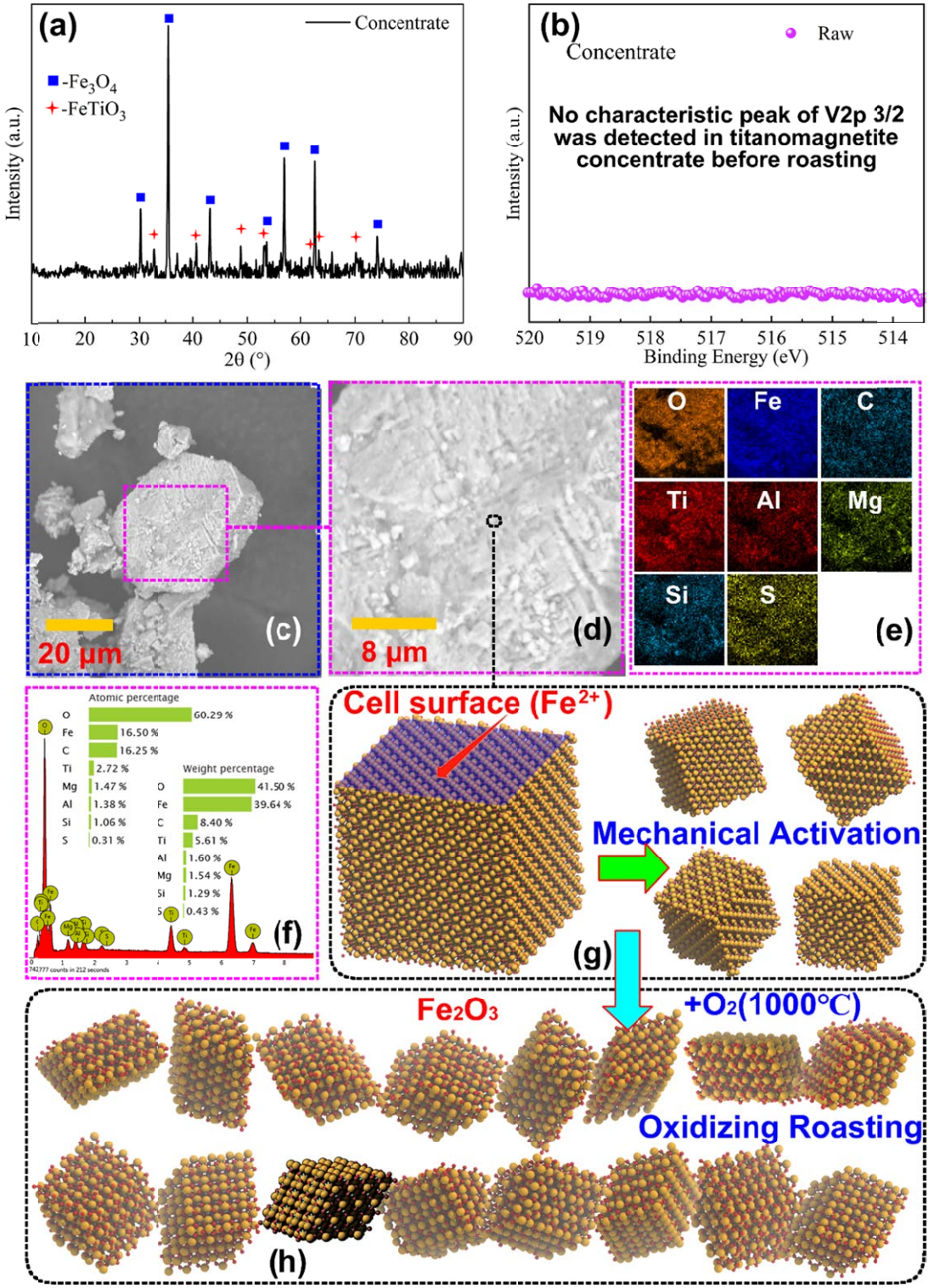


Fig. 1. XRD (a), XPS (b), SEM (c-f) characterization of titanomagnetite concentrate and schematic diagram of crystal structure transformation during oxidation roasting (g, h)

on the surface, exposure of divalent iron atoms could achieve lower surface energy. Fig. 1h illustrated the formation sites of $Fe_2O_3$ phase crystal particles during the oxidation process. Additionally, low-valent V elements exhibited poor acid solubility, necessitating an increase in their valence state to enhance leaching efficiency. The mineral phase reconstruction process of the titanomagnetite concentrate was typically achieved by mixing it with specific additives and subjecting it to oxidizing roasting conditions. This facilitated the lattice structure transformation of the primary phases ($Fe_3O_4$ to $Fe_2O_3$) while simultaneously striving to elevate the valence state of V (from $V^{3+}$ and $V^{4+}$ to $V_2O_5$) [18] to facilitate leaching.

TABLE 2

Chemical composition analysis of titanomagnetite concentrate

| Ore | TFe | $Fe_3O_4$ | $TiO_2$ | MgO | $SiO_2$ | $Al_2O_3$ | CaO | $V_2O_5$ | $Cr_2O_3$ |
|---|---|---|---|---|---|---|---|---|---|
| wt.% | 50.16 | 69.27 | 11.03 | 7.57 | 5.46 | 3.79 | 0.69 | 0.69 | 0.29 |

### 2.2. Oxidative roasting

Mineral phase reconstruction of titanomagnetite concentrate was conducted through oxidizing roasting, and samples were obtained by following different experimental procedures:

(1) Oxidized roasted sample OR: As shown in Fig. 2, Each time 50 g of the titanomagnetite concentrate was placed in a corundum crucible and roasted in batches in a muffle furnace at 900°C for 90 minutes. The resulting material was then crushed and prepared for subsequent leaching experiments.

(2) Oxidized roasted with magnesium compound sample ORx/y/z: Each time 50 g of titanomagnetite concentrate was mixed with 1-5 wt.% of x-MgO, y-$MgCO_3$, or z-$Mg(OH)_2$ powder, respectively. The mixtures were then roasted under the same conditions (900°C, 90 minutes) in batches. The resulting materials were crushed and prepared for subsequent control leaching experiments.

### 2.3. Leaching process

**(1) Leaching condition experiments**

The leaching operation process is illustrated in Fig. 3. A hydrochloric acid (a) leaching condition experiment was conducted with OR sample from the corundum crucible after oxidizing roasting of the titanomagnetite concentrate. Meanwhile, a sulfuric acid (b) control experiment was performed under the same conditions using another portion of the OR sample from

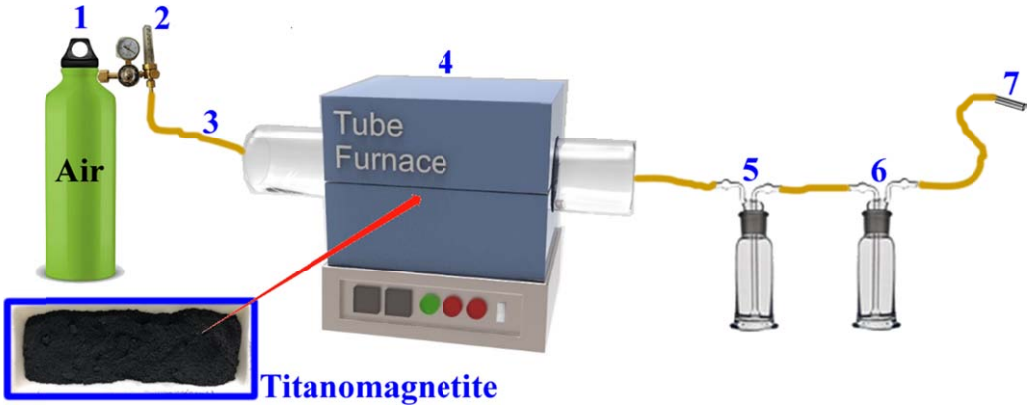


Fig. 2. Schematic diagram of the oxidative roasting experimental process. 1 – Drying air, 2 – Flowmeter (air flow rate 300 ml/min), 3 – Rubber hose, 4 – Tubular muffle furnace, 5 – Meng's washing bottle (anti backflow suction), 6 – Meng's washing bottle (water), 7 – Tail gas (discharged into the air)

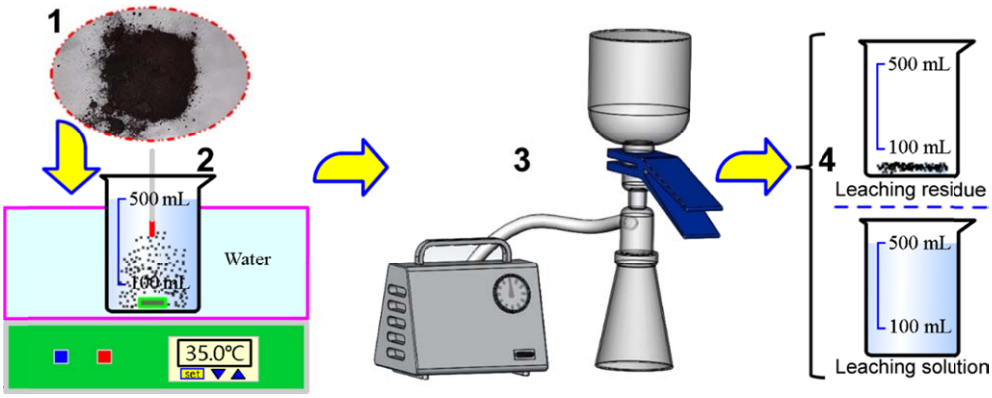


Fig. 3. Schematic diagram of the leaching experimental process. 1 – Material after oxidative roasting, 2 – Thermostat water bath, 3 – Vacuum suction filter, 4 – Separated leaching solution and leaching residue)

the crucible. The leachate and residue were separated using a Vacuum suction filter, and the resulting filtrate was diluted for ICP analysis to determine the vanadium ion concentration ($C_V$).

Specific experimental details were as follows:

The leaching time was set at 2 hours. As shown in TABLE 3, initially, the effect of acid concentration ($C$ = 0.5, 1, 1.5, 2, 2.5 mol/L) on the leaching efficiency was investigated at room temperature with a fixed liquid-to-solid ratio of 10:1 to determine the optimal acid concentration ($C_p$). Subsequently, the influence of leaching temperature ($T$ = 35, 55, 75, 95°C) on V leaching efficiency was explored while maintaining the liquid-to-solid ratio at 10:1 and the acid concentration at $C_p$ to establish the optimal leaching temperature ($T_p$). Finally, the impact of the liquid-to-solid ratio ($R_p$ = 4, 6, 8, 10) on V leaching efficiency was examined, with the acid concentration fixed at $C_p$ and the leaching temperature set at $T_p$, to ascertain the optimal liquid-to-solid ratio ($R_p$).

**(2) Leaching control experiments**

The leaching time was set at 2 hours. Under the optimal leaching conditions (acid concentration of $C_p$, leaching temperature of $T_p$, and liquid-to-solid ratio of $R_p$), control experiments were conducted using hydrochloric acid to leach the materials ORx/y/z from the corundum crucible after oxidizing roasting of the titanomagnetite concentrate. These experiments aimed to explore the effects of adding 0 wt.%, 1 wt.%, 2 wt.%, 3 wt.%, 4 wt.%, and 5 wt.% of x-MgO, y-$MgCO_3$, and z-$Mg(OH)_2$ powders on V leaching efficiency after oxidizing roasting (TABLE 4).

### 2.4. Determination of vanadium leaching efficiency

The leaching efficiency ($\eta$) was described by the ratio of the vanadium content in the leachate ($C_V$, g/kg) after leaching to the total vanadium content in the sample before leaching ($C_{TV}$, g/kg) for each set of samples (Eq. (1)). $C_V$ was determined by ICP-OES analysis of the diluted leachate, while $C_{TV}$ was measured through the following steps:

$$\eta = \frac{C_V}{C_{TV}} \tag{1}$$

(1) Using a polytetrafluoroethylene (PTFE) beaker as the container, 1 g of the titanomagnetite concentrate sample (accurate to 0.0005 g) after oxidizing roasting was completely dissolved by heating and boiling for 20 minutes in a mixture of 25 mL of nitric acid (68 wt.%), 25 mL of hydrofluoric acid, and 25 mL of hydrochloric acid (36 wt.%).

(2) After adding 25 mL of perchloric acid and heating until smoking at the beaker's rim, the sample of titanomagnetite concentrate was removed and allowed to cool. Subsequently, 25 mL of hydrochloric acid (1 + 1) was added to dissolve the salts.

(3) After filtering, the residue along with the filter paper underwent the same digestion process twice more.

(4) Finally, the filtrate was diluted to 500 ml with distilled water, and the vanadium concentration was analyzed and determined using inductively coupled plasma optical emission spectrometry (ICP-OES).

TABLE 3

Experimental design of leaching process – Effects of acid concentration, leaching temperature, and liquid-solid ratio on V leaching efficiency

| **No.** | **Control conditions** | **Fixed conditions** | | **Variable conditions** |
|---|---|---|---|---|
| | Type of acid | Leaching temperature °C | Liquid-to-solid ratio | Acid concentration mol/L |
| OR_Ca | a-Hydrochloric acid | Room temperature | 10:1 | 0.5-2.5 |
| OR_Cb | b-Sulfuric acid | Room temperature | 10:1 | 0.5-2.5 |
| **No.** | **Control conditions** | **Fixed conditions** | | **Variable conditions** |
| | Type of acid | Acid concentration mol/L | Liquid-to-solid ratio | Leaching temperature °C |
| OR_Ta | a-Hydrochloric acid | $C_p$ (optimal condition) | 10:1 | 35-95 |
| OR_Tb | b-Sulfuric acid | $C_p$ | 10:1 | 35-95 |
| **No.** | **Control conditions** | **Fixed conditions** | | **Variable conditions** |
| | Type of acid | Acid concentration mol/L | Leaching temperature °C | Liquid-to-solid ratio |
| OR_Ra | a-Hydrochloric acid | $C_p$ | $T_p$ (optimal condition) | 4-10 |
| OR_Rb | b-Sulfuric acid | $C_p$ | $T_p$ | 4-10 |

TABLE 4

Experimental design of leaching process-Effects of magnesium compound addition amount during roasting on leaching efficiency

| **No.** | **Fixed conditions** | **Variable conditions (Addition amount wt%)** | | |
|---|---|---|---|---|
| | Leaching conditions (HCl) | MgO | $MgCO_3$ | $Mg(OH)_2$ |
| ORx | $T_p$ +$C_p$ + $R_p$ | 0-5 | 0 | 0 |
| ORy | $T_p$ +$C_p$ + $R_p$ | 0 | 0-5 | 0 |
| ORz | $T_p$ +$C_p$ + $R_p$ | 0 | 0 | 0-5 |

### 2.5. Material characterization

The composition of the titanomagnetite concentrate raw material was determined through chemical analysis and Energy Dispersive X-ray Detector (EDX-LE ASSY CN ROHS, Shimadzu, Japan). The X-ray diffraction analysis (XRD, Rigaku D/MXA-3B with Cu Kα radiation at 40 kV and 40 mA) was used to identify the existence form of Fe phases before and after oxidizing roasting. X-ray photoelectron spectroscopy (XPS; Thermo K-Alpha+, Thermal Fisher) was employed to ascertain

the changes in the composition of V elements with different valences before and after oxidizing roasting. SEM (Phenom proX; Phenom) analysis was conducted to observe the morphological characteristics of the titanomagnetite concentrate before roasting, after roasting, and after leaching. Finally, the Inductively Coupled Plasma Optical Emission Spectrometry (ICP-OES, Leeman labs, America) analysis was utilized to determine the V content in the titanomagnetite concentrate raw material, pre-leaching samples, post-leaching filtrate, and the final products.

## 3. Results and discussion

### 3.1. Mneral phase reconstruction of titanomagnetite concentrate

Without adding magnesium compounds, the titanomagnetite concentrate could achieve two types of mineral phase reconstruction effects through oxidizing roasting: an increase in the valence of Fe elements ($Fe^{2+} \rightarrow Fe^{3+}$) and an increase in the valence of V elements ($V^{3+}$, $V^{4+} \rightarrow V_2O_5$).

$Fe^{2+} \rightarrow Fe^{3+}$: As shown in Fig. 4a, the XRD analysis results indicated that the main mineral phases in the titanomagnetite concentrate underwent a transformation from $Fe_3O_4$ and $FeTiO_3$ to $Fe_2O_3$ and $FeTi_2O_5$ after oxidizing roasting.

$V^{3+}$, $V^{4+} \rightarrow V_2O_5$: As shown in Figs. 4b and 4c [32], no characteristic peak of V2p 3/2 was detected in titanomagnetite concentrate, indicating that Fe was isomorphously substituted with V and low-valent V dispersed within the inverse spinel crystal structure of the concentrate. During the oxidative roasting process of titanomagnetite concentrate, the vanadium underwent a mineral phase reconstruction, transitioning from a low-valent state ($V^{3+}$) existing in isomorphic substitution with iron to a high-valent state ($V^{5+}$).

The purpose of mineral phase reconstruction was to enhance the leaching efficiency of vanadium. The increase in the valence state of iron elements actually corresponded to a transformation in the main crystal lattice structure of the mineral. This alteration in lattice structure was often accompanied by changes in volume. For titanomagnetite concentrate, the $Fe_3O_4$-like material, which was the primary phase, belonged to a face-centered cubic lattice structure with tightly arranged atoms. However, the $Fe_2O_3$ obtained after oxidation had a trigonal lattice structure with relatively loosely arranged atoms. As a result, the volume expanded after oxidation. Nevertheless, since the mineral phase reconstruction during oxidizing roasting occurred in a solid-state, the increase in volume did not disrupt the overall integrity of the lattice structure, nor did it create pore channels favorable for the subsequent leaching of high-valence vanadium oxides. Therefore, it was necessary to introduce active components during the oxidizing roasting process to modulate the lattice structure transformation during mineral phase reconstruction. This aspect, which involved the impact of magnesium compound addition on the vanadium leaching efficiency during oxidizing roasting, would be further discussed after determining the optimal leaching conditions.

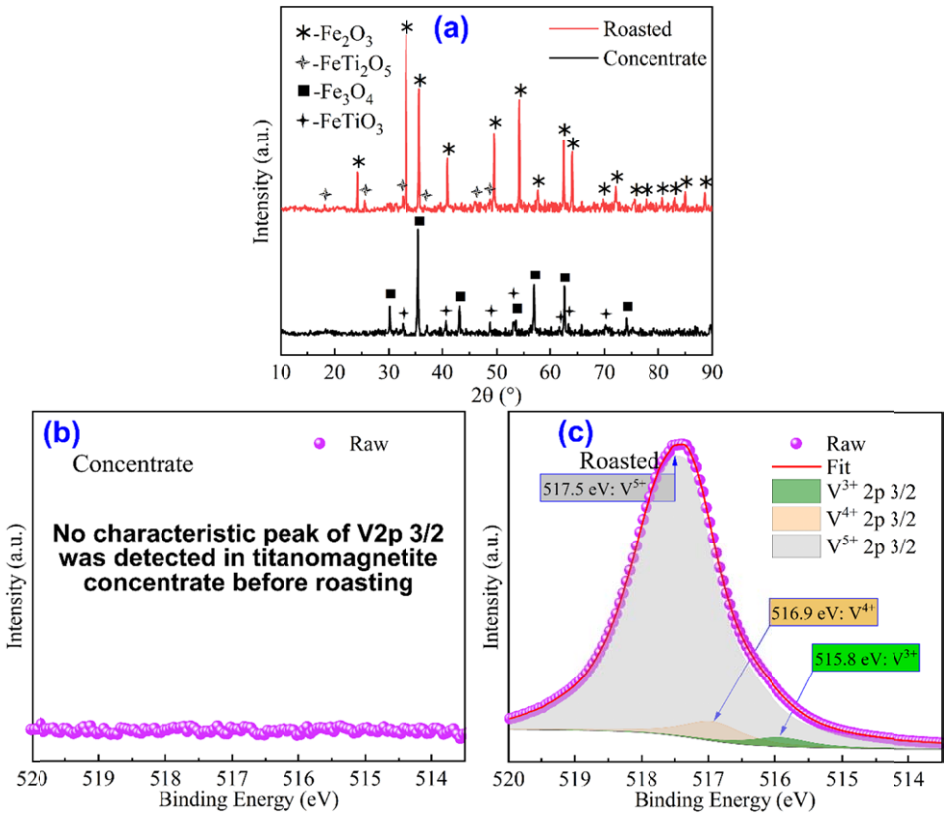


Fig. 4. XRD (a) characterization of titanomagnetite concentrate before and after roasting and XPS characterization of different valence V compositions before (b) and after roasting (c)

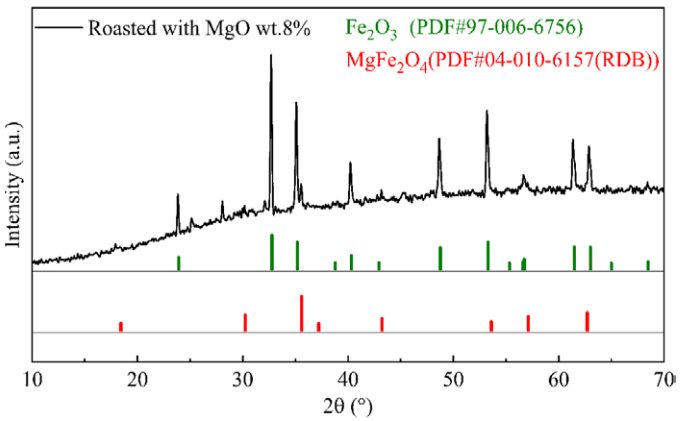


Fig. 5. XRD characterization of titanomagnetite concentrate roasted with MgO 8 wt.% for detecting $MgFe_2O_4$ phase

The difference after adding magnesium salt was that the $MgFe_2O_4$ phase forms during the oxidation process. In fact, with a small amount of MgO addition (Fig. 4a, 3 wt.% MgO, roasted in a muffle furnace at 900°C for 90 minutes) and under complete oxidation conditions, the $MgFe_2O_4$ phase was not detected. As shown in Fig. 5, keeping other conditions unchanged, when the MgO addition reached 8 wt.%, we detected the formation of the $MgFe_2O_4$ phase during the oxidative roasting process, which was beneficial for pore formation in the phase reconstruction process. Similar to $Fe_3O_4$, $MgFe_2O_4$ has an inverse spinel structure with a more compact lattice arrangement. During oxidation, it weakened the coverage and encapsulation of the $Fe_2O_3$ phase caused by the volume expansion resulting from the formation of loose lattice arrangement of $Fe_2O_3$, affecting the grain growth of the $Fe_2O_3$ phase. With an appropriate amount of MgO addition, it could even contract into pores, thereby enhancing the vanadium leaching process.

Titanomagnetite concentrate samples with different MgO additions (mass ratio 100:x (MgO), x = 0, 2, 4, 6, 8) were heated to 1100°C at a heating rate of 5°C/min in air atmosphere. The samples after oxidative roasting were characterized by SEM, with the results shown in Fig. 5. It can be seen that as the MgO addition increased, the microscopic morphology of the Titanomagnetite concentrate particle surface changes accordingly. When

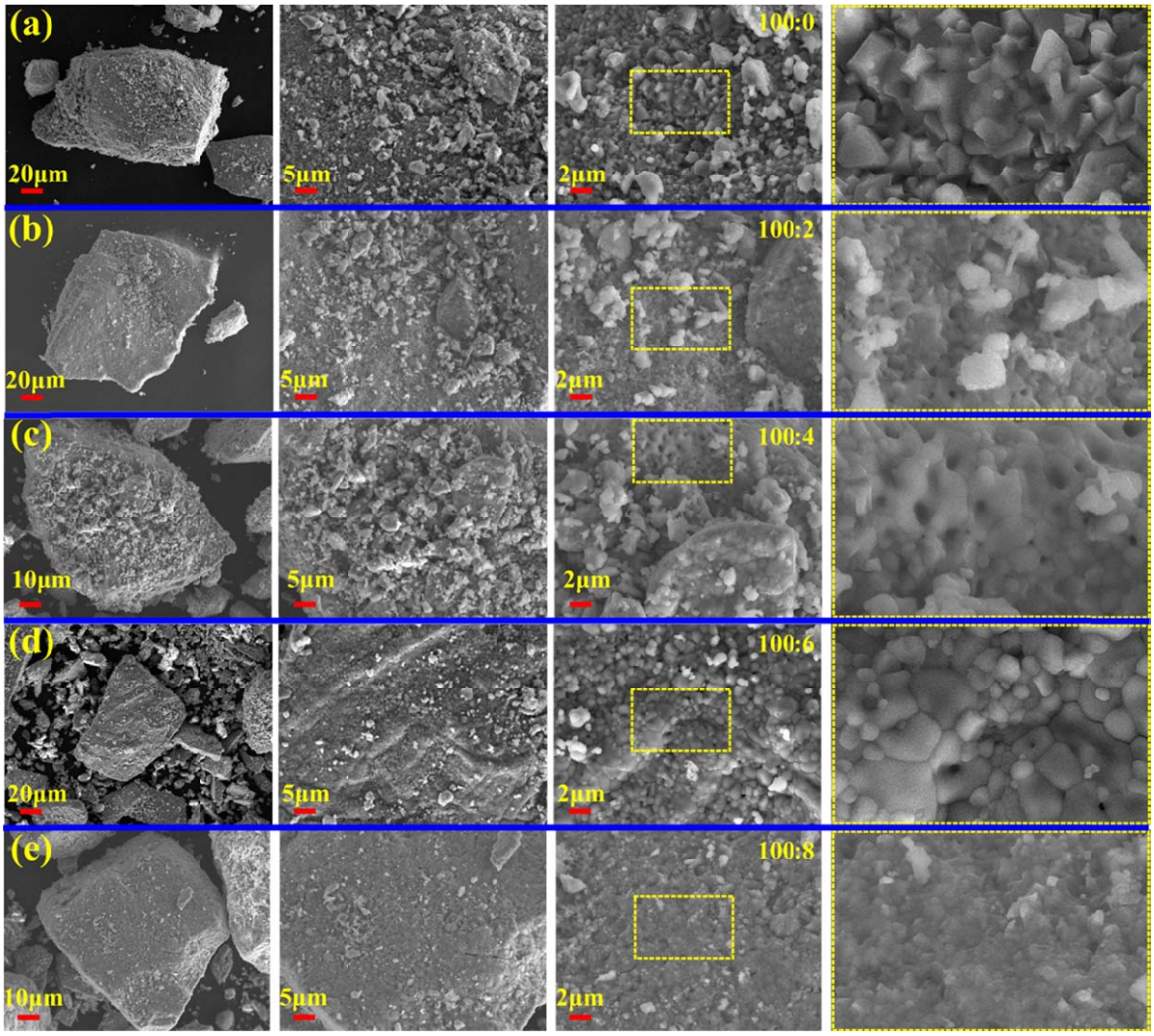


Fig. 6. SEM of pore formation characteristics on the surface of high valence iron oxide particles in titanomagnetite concentrate with different amounts of magnesium oxide addition (Titanomagnetite concentrate to magnesium oxide mass ratio a – 100:0, b – 100:2, c – 100:4, d – 100:6, e – 100:8)

the MgO addition was 100:0, the small grains of high-valence iron oxide had obvious edges and corners, with no pore formation. When the MgO addition was 100:2, micropores appeared on the surface of the high-valence iron oxide particles. When the MgO addition was 100:4, pore formation was significant. When the MgO addition was 100:6, pores were still formed, with clear grain boundaries. When the MgO addition was 100:8, no pores were detected. As the MgO addition increases, the pore formation phenomenon during the oxidative roasting of titanomagnetite concentrate exhibited a peak-like change. That was, after adding MgO (100:2), micropores appeared on the surface of high-valence iron oxide particles. When the mass ratio was 100:4, pore formation was most significant. Increasing the MgO addition to a mass ratio of 100:8 resulted in the disappearance of pore formation. Therefore, to promote pore formation on the surface of high-valence iron oxide during the oxidative roasting process and enhance the subsequent leaching process, the MgO addition could be uniformly controlled at 3 wt.%.

Pore formation phenomenon was related to the $MgFe_2O_4$ phase that appeared during the oxidation process. When this phase was evenly and appropriately dispersed on the surface of iron concentrate particles, it could delay the oxidation process, thereby limiting the growth rate of $Fe_2O_3$ grains and leading to local contraction and pore formation as shown in Fig. 7. However, when the $MgFe_2O_4$ phase was excessive, it instead formed overall small $Fe_2O_3$ grains, which collapsed and blocked the pore channels, severely affecting the pore formation effect.

Without MgO adding:

$$Fe_3O_4\text{-Cubic(FCC)} \xrightarrow{\text{Roasting}} Fe_2O_3\text{-Rhombohedral}$$

With MgO adding:

$$Fe_3O_4\text{-Cubic(FCC)} \xrightarrow{\text{Local}} MgFe_2O_4\text{-Cubic(FCC)} \xrightarrow{\text{Roasting}} Fe_2O_3\text{-Rhombohedral}$$

The addition of magnesium carbonate and magnesium hydroxide would have worse pore forming effect than directly adding magnesium oxide. This was because these two substances need to undergo decomposition reactions before obtaining magnesium oxide, making the pore forming mechanism (Fig. 6 and Fig. 7) of titanomagnetite concentrate oxidation roasting around active magnesium oxide sites more complex.

### 3.2. Vanadium leaching process from titanomagnetite concentrate after oxidative roasting

#### 3.2.1. The influence of leaching conditions and the amount of magnesium compounds added during roasting on the leaching efficiency of V

The leaching conditions of acid concentration, temperature, and liquid-to-solid radio were tested according to TABLE 3, and the results obtained are shown in Fig. 8a-c.

**The influence of acid concentration on vanadium leaching efficiency:** Hydrochloric acid is an aqueous solution of hydrogen chloride gas, which has strong acidity. Its leaching ability is almost proportional to its concentration under low concentration conditions. However, high concentration hydrochloric acid is prone to volatilization, especially at high temperatures,

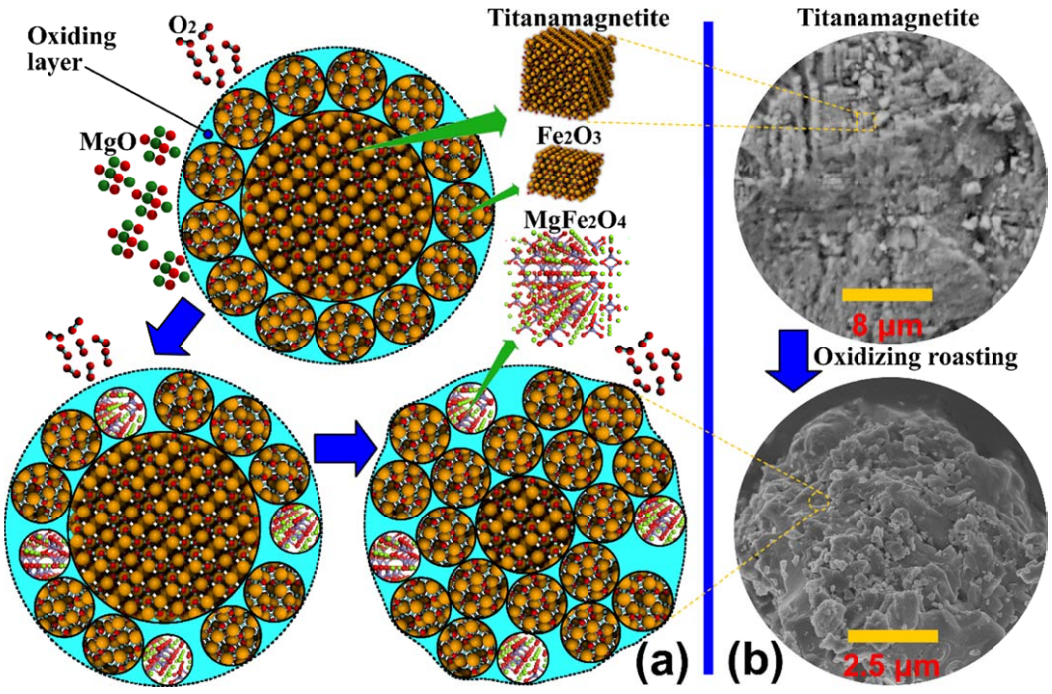


Fig. 7. Analysis of pore formation mechanism due to local lattice structure shrinkage caused by MgO during the mineral phase reconstruction of titanomagnetite concentrate through oxidative roasting (a), and SEM microscopic morphology analysis of titanomagnetite concentrate before and after oxidative roasting (b)

which may lead to equipment corrosion and environmental pollution. Therefore, low concentration hydrochloric acid of no more than 4mol/L is usually used in the leaching process.

Sulfuric acid is a hydrate of sulfur trioxide, which has strong acidity and good thermal stability. It could be used under higher leaching temperature conditions. The sulfate produced during the leaching process would affect the leaching effect of sulfuric acid.

Under the same concentration conditions, sulfuric acid, as a dibasic acid, would achieve better leaching effect than hydrochloric acid [33,34]. However, during the sulfuric acid leaching process, sulfate would be introduced into titanomagnetite concentrate, which required subsequent desulfurization treatment; When the acid concentration increased, the leaching rate of vanadium reached a peak (Fig. 8a), indicating that other metal elements such as iron would affect the effective acid concentration that actually acted on the vanadium leaching [35].

As illustrated in Fig. 8a, different acid type led to distinct patterns in vanadium leaching efficiency. Although the vanadium leaching efficiency generally increased initially and then decreased with rising acid concentration, there were notable differences between hydrochloric and sulfuric acid. Specifically, the increase in vanadium leaching efficiency with hydrochloric acid concentration up to 1.5 mol/L was more significant than that with sulfuric acid. However, beyond 1.5 mol/L, the decrease in vanadium leaching efficiency due to increased hydrochloric acid concentration was less pronounced compared to sulfuric acid. This phenomenon was inherently linked to the actual $H^+$ concentration available for reaction with vanadium oxides within different acid leaching systems. Initially, as the $H^+$ concentration increased, the availability of $H^+$ for reaction with vanadium oxides also rose, leading to a positive correlation between vanadium leaching efficiency and acid concentration up to a certain range (0-1.5 mol/L). Nevertheless, at higher acid concentrations, the participation of additional metal oxides (non-vanadium) in the leaching process increased, consuming $H^+$ ions and effectively reducing the concentration available for reaction with vanadium oxides. This resulted in a negative correlation between vanadium leaching efficiency and acid concentration. Moreover, due to the distinct chemical properties of hydrochloric acid (a monoprotic acid) and sulfuric acid (a diprotic acid), the influence of hydrochloric acid on the vanadium leaching efficiency exhibited a certain degree of lag compared to sulfuric acid. According to Fig. 8a, the optimal acid concentration for vanadium leaching using both acids was $C_p$ = 1.5 mol/L when dealing with titanomagnetite concentrate.

**The influence of temperature on vanadium leaching efficiency:** As evident from Fig. 8b, the vanadium leaching efficiency increased with rising temperature. However, the magnitude of this increase was more significant in the sulfuric acid leaching process compared to the hydrochloric acid process. This observation could be attributed to the stronger volatility and reducibility of hydrochloric acid. As temperature increased, it facilitated the relevant reactions in the leaching process. However, it also led to increased evaporation of hydrochloric acid. Additionally, being

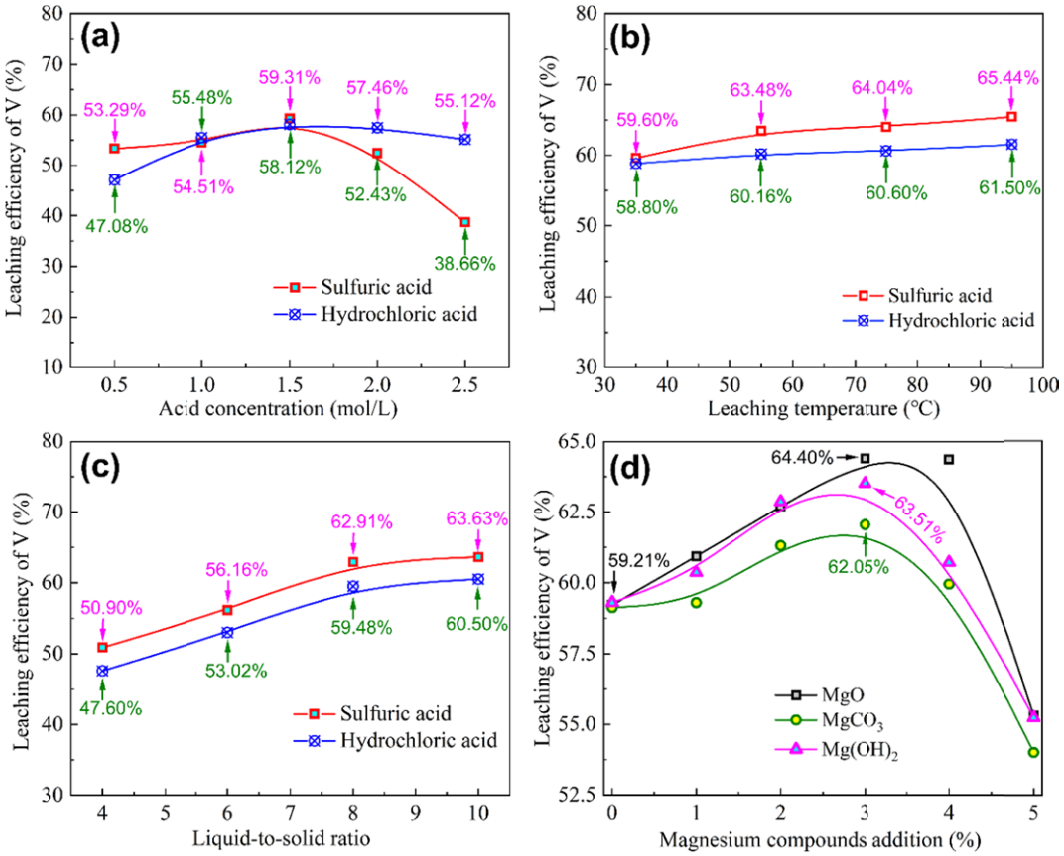


Fig. 8. Effects of acid concentration (a), leaching temperature (b), liquid-solid ratio (c), and the amount of magnesium compound added during roasting (d) on the leaching efficiency (experimental conditions were shown in TABLE 3 and 4)

a reducing acid, hydrochloric acid reacted with some vanadium oxides, generating chlorine gas and lower-valent vanadium ions. This reaction reduced the concentration of $H^+$ ions available for reaction with vanadium oxides, thereby partially offsetting the beneficial effect of temperature on the vanadium leaching efficiency. On the other hand, sulfuric acid lacks both volatility and reducibility, explaining why the increase in temperature had a more pronounced effect on the vanadium leaching efficiency in the sulfuric acid process. After considering the competing effects of hydrochloric acid's volatility, reducibility, and the beneficial impact of increased temperature on the reactions, the optimal leaching temperature for hydrochloric acid was determined to be $T_p$ = 55°C. At this temperature, sulfuric acid also exhibited good vanadium leaching efficiency, and further increases in temperature did not significantly enhance the results. Therefore, it could be concluded that the optimal leaching temperature for both sulfuric acid and hydrochloric acid, when dealing with titanomagnetite concentrate, was $T_p$ = 55°C.

**The influence of liquid-to-solid ratio on vanadium leaching efficiency:** As indicated by the results presented in Fig. 8c, the leaching efficiency of vanadium using sulfuric acid (diprotic acid) was approximately 3% higher than that achieved with hydrochloric acid (monoprotic acid). For both acids, the vanadium leaching efficiency increased with the liquid-to-solid ratio. However, once the liquid-to-solid ratio reached 8, the vanadium leaching efficiency stabilized. Therefore, it could be concluded that the optimal liquid-to-solid ratio for both sulfuric acid and hydrochloric acid, when dealing with titanomagnetite concentrate, was $R_p$ = 8.

The influence of magnesium compound addition on vanadium leaching efficiency during roasting: Leaching experiments were conducted according to TABLE 4, and the results were presented in Fig. 8d. It could be observed that the addition of appropriate amounts of magnesium compounds could enhance the vanadium leaching efficiency. Among the tested compounds, the direct addition of MgO proved to be the most effective. This was because during the oxidation roasting process (Fig. 8a), highly active MgO reacts with trigonal $Fe_2O_3$ to form $MgFe_2O_4$, which also exhibits a face-centered cubic lattice structure. This reaction alters the lattice structure transformation pattern during mineral phase reconstruction, shifting from a solely expansive lattice structure transformation to a mixed mode of overall expansion and local contraction. This adjustment in the lattice structure transformation pattern positively impacts the vanadium leaching efficiency from titanomagnetite concentrate:

The addition of magnesium compounds facilitated the formation of pore channels (Fig. 7b) beneficial for the subsequent leaching process, thereby improving the leaching efficiency of vanadium. All three magnesium compounds exhibited their best leaching results at a 3 wt.% addition level. Under these conditions, MgO, $MgCO_3$, and $Mg(OH)_2$ enhanced the vanadium leaching efficiency by 5.19%, 2.92%, and 4.21%, respectively (Fig. 8d). In fact, both $MgCO_3$ and $Mg(OH)_2$ underwent decomposition reactions to produce MgO. However, these compounds would react with other substances before decomposition or decompose incompletely, resulting in a reduced activity of MgO that ultimately affected the transformation of $Fe_2O_3$'s lattice structure and, consequently, the decrease of the vanadium leaching efficiency. When the addition of magnesium compounds was further increased (>3 wt.%), the local reaction between MgO and $Fe_2O_3$ intensified, potentially collapsing and forming $MgFe_2O_4$ phases that cover pore structures. This could encapsulate the vanadium inside mineral particles, leading to a decreased vanadium leaching efficiency.

### 3.2.2. Analysis of vanadium leaching mechanism

Before the oxidation process, vanadium exists in the titanium magnetite concentrate in the form of a spinel structure of $FeO{\cdot}V_2O_3$. As the oxidation process intensifies, the spinel lattice structure is disrupted, and vanadium transitions from a trivalent

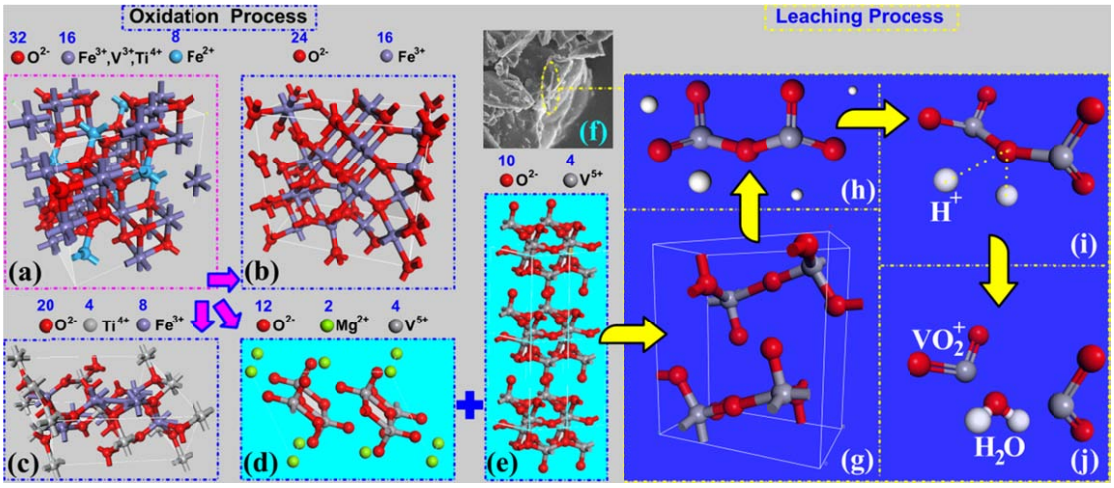


Fig. 9. The migration and corresponding phases (forms) of vanadium in oxidation process and leaching process of titanomagnetite concentrate. (a – lattice structure of titanomagnetite concentrate; b – lattice structure of $Fe_2O_3$; c – lattice structure of $Fe_2TiO_5$; d – lattice structure of $Mg_2VO_6$; e – lattice structure of $V_2O_5$; f – SEM morphology characterization of titanomagnetite concentrate during the leaching process; g – single crystal cell of $V_2O_5$; h,i,j – $V_2O_5$ unit cell structure decomposition in acid solution)

to a pentavalent state. The liberated pentavalent vanadium partly reacts with magnesium oxide to form $Mg_2VO_6$, while another portion directly forms $V_2O_5$ (Fig. 9a-e). After oxidation roasting, most of the vanadium participated in the leaching process in the form of high-valent oxide ($V_2O_5$), possibly exhibiting dendritic or lamellar phase structures (Fig. 9f) [36]. In dilute hydrochloric acid/sulfuric acid, the $V_2O_5$ crystal possesses an orthorhombic structure, and on its surface, the oxygen atoms between two vanadium atoms would react with $H^+$ to produce water. This reaction caused the gradual decomposition of the $V_2O_5$ crystal, resulting in the presence of $VO_2^+$ ions in the leach solution (Fig. 9h-j, Eq. (2)). When concentrated hydrochloric acid (>4 mol/L) was used for leaching, partial $VO_2^+$ ions further reacted with the acid to generate $VO_2^+$ and $Cl_2$ (Eq. (3)).

$$V_2O_5 + 2H^+ = 2VO_2^+ + H_2O \quad (2)$$

$$VO_2^+ + 2HCl\ (>4\ mol/L) = VO^{2+} + Cl_2(g) + H_2O \quad (3)$$

The form of vanadium ions in the leaching solution was greatly influenced by the pH value of the system, as evident from the reactions presented in TABLE 5 [37,38]. Disregarding the effects of other impurity ions, it was possible to calculate the variation of the concentrations of 12 vanadium-related ions in the V-$H_2O$ system with pH using the 11 reactions and their equilibrium constants provided in TABLE 5. Fig. 10 illustrates the results of these calculations, showing how the concentrations of these 12 ions changed with pH under room temperature conditions in the leaching process of vanadium from titanomagnetite concentrate.

As shown in Fig. 10, under low pH conditions (pH < 0.9), most of the vanadium existed in the form of $VO_2^+$. With increasing pH, 7 distinct pH range transitions occurred for different vanadium ion species:

pH = 0.9-2.6: $VO_2^+ \rightarrow H_2V_{10}O_{28}^{4-}$;

pH = 2.6-4.8: $H_2V_{10}O_{28}^{4-} \rightarrow HV_{10}O_{28}^{5-}$;

TABLE 5

Reaction equations and corresponding equilibrium constants of related ions in the V-$H_2O$ system at room temperature [37,38]

| No. | Ionic reaction equations | Equilibrium constants (lgK) |
|---|---|---|
| 1 | $VO_4^{3-} + H^+ = 2HVO_4^{2-}$ | 13.36 |
| 2 | $VO_4^{3-} + 2H^+ = H_2VO_4^{2-}$ | 21.31 |
| 3 | $2VO_4^{3-} + 2H^+ = V_2O_7^{4-} + H_2O$ | 27.38 |
| 4 | $2VO_4^{3-} + 3H^+ = HV_2O_7^{3-} + H_2O$ | 37.17 |
| 5 | $2VO_4^{3-} + 4H^+ = H_2V_2O_7^{2-} + H_2O$ | 45.4 |
| 6 | $4VO_4^{3-} + 8H^+ = V_4O_{12}^{4-} + 4H_2O$ | 95.11 |
| 7 | $5VO_4^{3-} + 10H^+ = V_5O_{15}^{5-} + 5H_2O$ | 118.69 |
| 8 | $10VO_4^{3-} + 24H^+ = V_{10}O_{28}^{6-} + 12H_2O$ | 264.82 |
| 9 | $10VO_4^{3-} + 25H^+ = HV_{10}O_{28}^{5-} + 12H_2O$ | 270.89 |
| 10 | $10VO_4^{3-} + 26H^+ = H_2V_{10}O_{28}^{4-} + 12H_2O$ | 274.49 |
| 11 | $VO_4^{3-} + 4H^+ = VO_2^+ + 2H_2O$ | 28.23 |

pH = 4.8-6.0: $HV_{10}O_{28}^{5-} \rightarrow V_{10}O_{28}^{6-} + V_4O_{12}^{4-}$

pH = 6.0-8.0: $V_{10}O_{28}^{6-} \rightarrow V_4O_{12}^{4-} + V_5O_{15}^{5-} +$
$+ H_2V_2O_7^{2-} + H_2VO_4^{2-}$

pH = 8.0-9.7: $V_4O_{12}^{4-} + V_5O_{15}^{5-} + H_2V_2O_7^{2-} +$
$+ H_2VO_4^{2-} \rightarrow HVO_4^{2-} + HV_2O_7^{3-} + V_2O_7^{4-}$

pH = 9.7-11.4: $HV_2O_7^{3-} \rightarrow HVO_4^{2-} + V_2O_7^{4-}$

pH = 11.4-14: $HVO_4^{2-} + V_2O_7^{4-} \rightarrow VO_4^{3-}$

In fact, at pH 6, the primary non-hydrogen large ion in the system, $V_{10}O_{28}^{6-}$, accounted for 31.4% of the vanadium content, making it more prone to precipitation from the system. This ion formed within a pH range of 5-6.3, which could be considered as the pH range for vanadium precipitation in the V-$H_2O$ system. In the presence of other impurity ions, this range might experience slight fluctuations, necessitating further studies on the vanadium precipitation process to determine the specific pH range for separation from other metal ions when processing titanomagnetite concentrate.

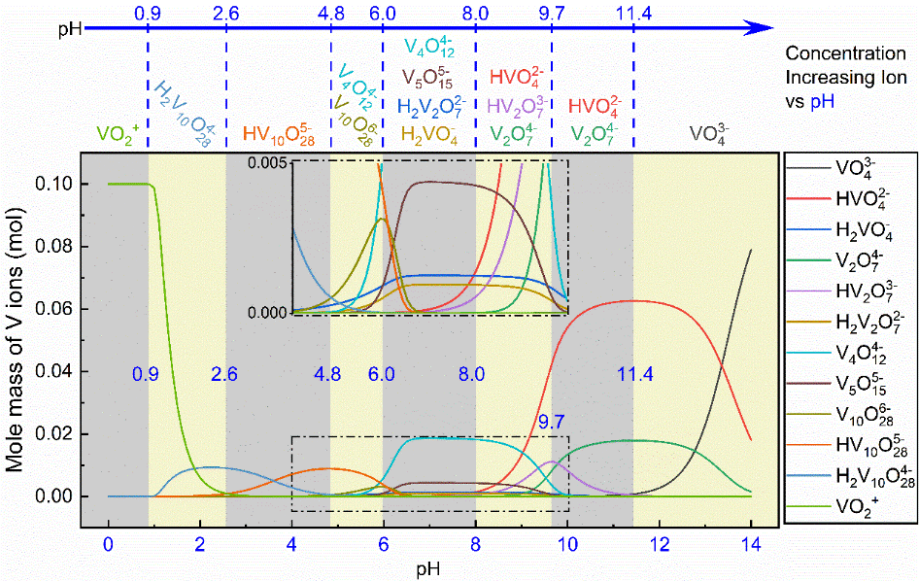


Fig. 10. Calculation results of the variation of 12 V-related ion concentrations with pH in the V-$H_2O$ system at room temperature

### 3.3. Direct vanadium extraction process from titanomagnetite concentrate

The direct vanadium extraction process, as depicted in Fig. 11, consisted of four main steps: oxidation roasting, leaching, vanadium precipitation, and calcination. During the oxidation roasting process, the addition of MgO facilitated a mineral phase reconstruction process that altered the crystal structure of the titanomagnetite concentrate. This not only increased the valence states of Fe and V elements but also created porous channels beneficial for subsequent leaching. The primary factors influencing the leaching process included acid concentration ($C_p$ = 1.5 mol/L), leaching temperature ($T_p$ = 55°C), and liquid-to-solid ratio ($R_p$ = 8). Furthermore, different types of acids, such as HCl and $H_2SO_4$, exhibited slight variations in their specific modes of action during the leaching process. These variations were primarily attributed to the reducing properties, volatility, and $H^+$-releasing capabilities of the acids (monoprotic or diprotic). Future research could delve into the kinetics of the leaching process, as well as the processes of vanadium precipitation and calcination.

The final product of the direct vanadium extraction process was $V_2O_5$ at 96% purity. After leaching, the resulting leach residue could undergo direct reduction and magnetic separation to produce direct reduced iron and titanium slag with a $TiO_2$ grade of approximately 40%. This approach allowed for the comprehensive recovery and utilization of iron, vanadium, and titanium from titanomagnetite concentrate.

## 4. Conclusion

The oxidation roasting and leaching processes in the direct vanadium extraction from titanomagnetite concentrate were investigated. The main conclusions are as follows:

(1) During the process of oxidation roasting, the addition of MgO altered the lattice structure transformation mode in the mineral phase reconstruction process. It shifted from a single expansive lattice structure transformation mode to a hybrid mode of overall expansion and local contraction:
Without MgO adding:

$$Fe_3O_4\text{-Cubic(FCC)} \xrightarrow{\text{Roasting}} Fe_2O_3\text{-Rhombohedral}$$

With MgO adding:

$$Fe_3O_4\text{-Cubic(FCC)} \xrightarrow{\text{Local}} MgFe_2O_4\text{-Cubic(FCC)} \xrightarrow{\text{Roasting}} Fe_2O_3\text{-Rhombohedral}$$

Which resulted in the formation of porous channels that facilitated the subsequent leaching process of the titanomagnetite concentrate.

(2) While HCl and $H_2SO_4$, two different types of acids, exhibited slight variations in their specific modes of action during the leaching process of titanomagnetite concentrate, their overall effects were consistent. The reasons for these variations were primarily related to the reducing properties, volatility, and $H^+$-releasing capabilities of the acids (monoprotic/diprotic). When the leaching time was set at 2 hours,

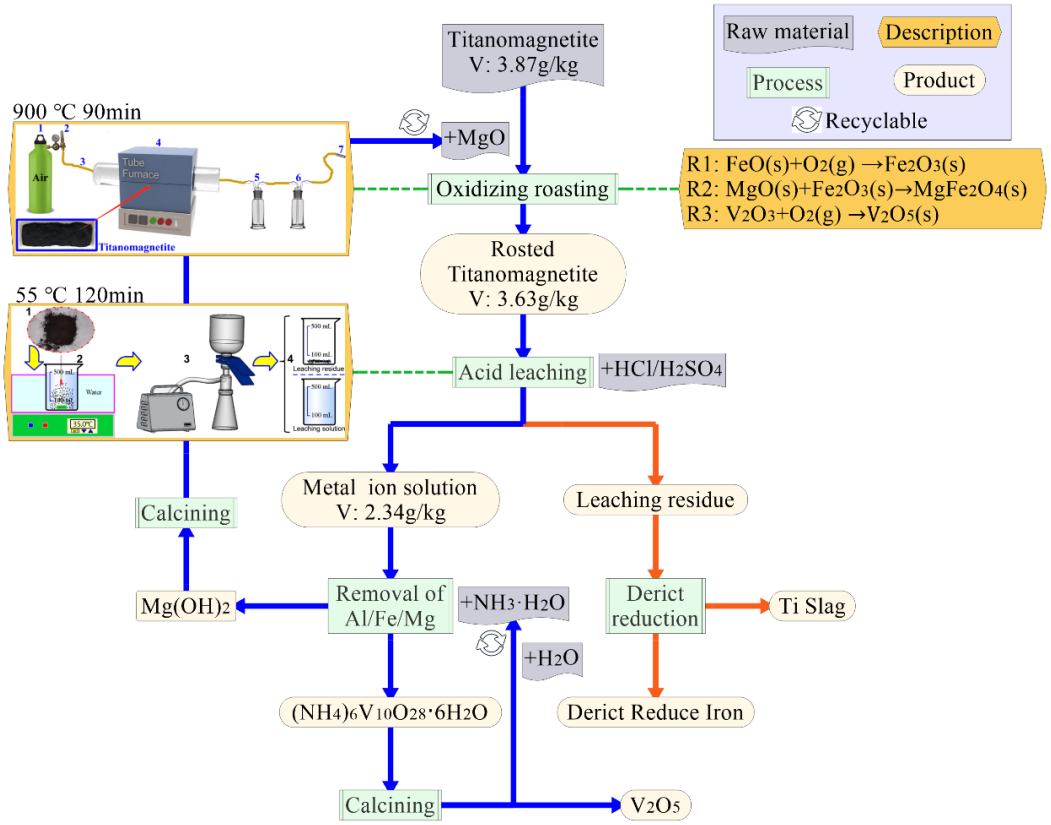


Fig. 11. Direct vanadium extraction process from titanomagnetite concentrate

the optimal leaching conditions for both hydrochloric acid and sulfuric acid were found to be: acid concentration ($C_p$) of 1.5 mol/L, leaching temperature ($T_p$) of 55°C, and liquid-to-solid ratio ($R_p$) of 8. Under these conditions, the vanadium leaching efficiency reached 64.40% when using hydrochloric acid to leach the MgO-added titanomagnetite concentrate that underwent mineral phase reconstruction through oxidation roasting.

(3) During the leaching process of titanomagnetite concentrate, the oxygen atoms between the V atoms on the surface of $V_2O_5$ crystals would react with $H^+$ ions to produce water, causing the gradual decomposition of $V_2O_5$ crystals. As a result, vanadium would exist in the leaching solution in the form of $VO_2^+$ ions. Calculations of the changes in concentration of 12 V-related ions in the V-$H_2O$ system with varying pH values showed that when the pH was 6, the main H-free large ion in the system, $V_{10}O_{28}^{6-}$, accounted for 31.4% of the total V content, making it easier to precipitate out of the system. The pH range for the formation of this ion was determined to be 5-6.3, which could be considered as the pH range for vanadium precipitation in the V-$H_2O$ system.

**Acknowledgments**

This work was supported by the project of Panxi Strategic Resource Innovation and Development (LB-SK-HT23-0432), the Opening Project of Sichuan Provincial Key Laboratory of Material Corrosion and Protection (2022CL31), and the Opening Project of Key Laboratory of Green Chemistry of Sichuan Institutes of Higher Education (LYJ2102).

## REFERENCES

[1] G. Yang, X. Sun, Z. Li, X. Li, Q. Yong, Effects of vanadium on the microstructure and mechanical properties of a high strength low alloy martensite steel. Mater. Design **50** (1), 102-107 (2013). DOI: https://doi.org/10.1016/j.matdes.2013.03.019

[2] M. Imtiaz, M.S. Rizwan, S. Xiong, H. Li, M. Ashraf, S.M. Shahzad, M. Shahzad, M. Rizwan, S. Tu, Vanadium, recent advancements and research prospects: A review. Environment International **80** (1), 79-88 (2015). DOI: https://doi.org/10.1016/j.envint.2015.03.018

[3] Y. Zhang, S. Bao, T. Liu, T. Chen, J. Huang, The technology of extracting vanadium from stone coal in China: History, current status and future prospects. Hydrometallurgy **109** (1), 116-124 (2011). DOI: https://doi.org/10.1016/j.hydromet.2011.06.002

[4] D. He, Q. Feng, G. Zhang, L. Ou, Y. Lu, An environmentally-friendly technology of vanadium extraction from stone coal. Minerals Engineering **20** (12), 1184-1186 (2007). DOI: https://doi.org/10.1016/j.mineng.2007.04.017

[5] Q. Zhang, Y. Zhao, G. Yuan, W. Yang, The effect of vanadium on microstructure and mechanical properties of Fe-based high-strength alloys. Results in Physics **15** (1), 102335 (2019). DOI: https://doi.org/10.1016/j.rinp.2019.102335

[6] C. Choi, S. Kim, R. Kim, Y. Choi, S. Kim, H.Y. Jung, J.H. Yang, H.T. Kim, A review of vanadium electrolytes for vanadium redox flow batteries, Renew. Sust. Energ. Rev. **69** (1), 263-274 (2017). DOI: https://doi.org/10.1016/j.rser.2016.11.188

[7] R. Moskalyk, A. Alfantazi, Processing of vanadium: a review. Minerals Engineering **16** (9), 793-805 (2003). DOI: https://doi.org/10.1016/S0892-6875(03)00213-9

[8] Y. Wu, D. Chen, W. Liu, Z. Sun, B. Zhang, Global vanadium industry development report 2020. Iron Steel Vanadium Titanium **5** (1), 1-9 (2021). (In Chinese).

[9] Y. Wu, D. Chen, W. Liu, Z. Sun, B. Zhang, R. He, Global vanadium industry development report 2021. Iron Steel Vanadium Titanium **43** (1), 1-9 (2022). (In Chinese).

[10] S. Mironov, Y.S. Sato, H. Kokawa, Friction-stir welding and processing of Ti-6Al-4V titanium alloy: A review. J. Mater. Sci. Technol. **34** (1), 58-72 (2018). DOI: https://doi.org/10.1016/j.jmst.2017.10.018

[11] J. Li, X. Zhou, M. Brochu, N. Provatas, Y. Zhao, Solidification microstructure simulation of Ti-6Al-4V in metal additive manufacturing: A review. Additive Manufacturing **29** (1), 1-14 (2020). DOI: https://doi.org/10.1016/j.addma.2019.100989

[12] Q. Sun, L. Wang, R. Cheng, Z. Liu, X. He, N. Zhao, B. Liu, A Novel $SiO_2$-Supported Fluorine Modified Chromium-Vanadium Bimetallic Catalyst for Ethylene Polymerization and Ethylene/1-Hexene Copolymerization. Macromol. React. Eng. **55** (1), 1-12 (2017). DOI: https://doi.org/10.1002/mren.201600055

[13] W. Wang, Q. Luo, B. Li, X. Wei, L. Li, Z. Yang, Recent progress in redox flow battery research and development. Adv. Funct. Mater. **23** (8), 970-86 (2013). DOI: https://doi.org/10.1002/adfm.201200694

[14] M. Skyllas-Kazacos, G. Kazacos, G. Poon, H. Verseema, Recent advances with UNSW vanadium-based redox flow batteries. Int. J. Energ. Res. **34** (2), 182-189 (2010). DOI: https://doi.org/10.1002/er.1658

[15] M. Skyllas-Kazacos, L. Cao, M. Kazacos, N. Kausar, A. Mousa, Vanadium electrolyte studies for the vanadium redox battery-a review. ChemSusChem **9** (1), 1521-1543 (2016). DOI: https://doi.org/10.1002/cssc.201600102

[16] C. Lv, K. Yang, S. Wen, S. Bai, Q. Feng, A new technique for preparation of high-grade titanium slag from titanomagnetite concentrate by reduction-melting-magnetic separation processing. JOM **69** (1), 1801-1805 (2017). DOI: https://doi.org/10.1007/s11837-017-2507-3

[17] H. Lv, M. Wu, Z. Zhang, X. Wu, L. Li, Z. Gao, Co-precipitation behaviour of titanium-containing silicate solution. Chemical Papers **70** (1), 1632-1641 (2016). DOI: https://doi.org/10.1515/chempap-2016-0100

[18] J. He, X. Jiang, H. Ji, Y. Jin, Z. Zhang, F. Shen, Research progress on direct extraction of vanadium from vanadium titanium magnetite. China Metallurgy **33** (3), 29-38 (2023). (In Chinese).

[19] Y. Liu, F. Meng, F. Fang, W. Wang, J. Chu, T. Qi, Preparation of rutile titanium dioxide pigment from low-grade titanium slag pretreated by the NaOH molten salt method. Dyes and Pigments **125** (1), 384-391 (2016). DOI: https://doi.org/10.1016/j.dyepig.2015.10.036

[20] D. Chen, L. Zhao, Y. Liu, T. Qi, J. Wang, L. Wang, A novel process for recovery of iron, titanium, and vanadium from titanomagnetite concentrates: NaOH molten salt roasting and water leaching processes. J. Hazard Mater. **244-245** (1), 588-595 (2013). DOI: https://doi.org/10.1016/j.jhazmat.2012.10.052

[21] Y. Sui, Y. Guo, A. Travyanov, T. Jiang, F. Chen, G. Qiu, Reduction roasting-magnetic separation of vanadium tailings in presence of sodium sulfate and its mechanisms. Rare Metals **35** (1), 954-960 (2016). (In Chinese).

[22] Y. Zhang, L. Yi, L. Wang, D. Chen, W. Wang, Y. Liu, H. Zhao, T. Qi, A novel process for the recovery of iron, titanium, and vanadium from vanadium-bearing titanomagnetite: sodium modification–direct reduction coupled process. Int. J. Min. Met. Mater. **24** (1), 504-11 (2017). DOI: https://doi.org/10.1007/s12613-017-1431-4

[23] X. Luo, H. Dong, S. Zhang, Y. Liu, Study on the sodium oxidation properties of low-iron vanadium-titanium magnetite with high vanadium and titanium. Energy Sources, Part A: Recovery, Utilization, and Environmental Effects **40** (17), 1998-2008 (2018). DOI: https://doi.org/10.1080/15567036.2018.1486907

[24] S. Zhang, G. Li, R. Xiao, J. Luo, L. Yi, M. Rao, Extraction of vanadium from low-vanadium grade magnetite concentrate pellets with sodium salt. Journal of Materials Research and Technology **15**, 5712-5722 (2021). DOI: https://doi.org/10.1016/j.jmrt.2021.11.039

[25] Y. Luo, X. Che, X. Cui, Q. Zheng, L. Wang, Selective leaching of vanadium from V-Ti magnetite concentrates by pellet calcification roasting-$H_2SO_4$ leaching process. International Journal of Mining Science and Technology **31** (3), 507-513 (2021). DOI: https://doi.org/10.1016/j.ijmst.2021.02.002

[26] Z. Wang, Z. Peng, Y. Li, Y. Zhu, K. Xie, Selective sulfuric acid cyclic leaching of vanadium from the calcification roasting pellets of vanadium titanomagnetite. Journal of Materials Research and Technology **23** (0), 778-790 (2023). DOI: https://doi.org/10.1016/j.jmrt.2023.01.046

[27] F. Gao, H. Du, S. Wang, B. Chen, J. Li, Y. Zhang, M. Li, B. Liu, A.U. Olayiwola, A comparative study of extracting vanadium from vanadium titano-magnetite ores: Calcium salt roasting vs sodium salt roasting. Mineral Processing and Extractive Metallurgy Review **44** (5), 352-364 (2022). DOI: https://doi.org/10.1080/08827508.2022.2069105

[28] J. Wen, T. Jiang, Y. Liu, X. Xue, Extraction behavior of vanadium and chromium by calcification roasting-acid leaching from high chromium vanadium slag: optimization using response surface methodology. Metallurgy Review **40** (1), 56-66 (2018). DOI: https://doi.org/10.1080/08827508.2018.1481059

[29] G.B. Sadykhov, K.V. Goncharov, T.V. Goncharenko, T.V. Olyunina, Phase transformations during the oxidation of calcium-containing titanium-vanadium slags and their influence on the formation of calcium vanadates. Russian Metallurgy (Metally) **2013** (3), 161-168 (2013). DOI: https://doi.org/10.1134/s0036029513030105

[30] T. Wang, L. Xu, C. Liu, Z. Zhang, Calcified roasting-acid leaching process of vanadium from low-grade vanadium-containing stone coal. Chinese Journal of Geochemistry **33** (2), 163-167 (2014). DOI: https://doi.org/10.1007/s11631-014-0672-4

[31] H.Y. Li, C.J. Wang, Y.H. Yuan, Y. Guo, J. Diao, B. Xie, Magnesiation roasting-acid leaching: a zero-discharge method for vanadium extraction from vanadium slag. Journal of Cleaner Production **260** (0), 121091-121091 (2020). DOI: https://doi.org/10.1016/j.jclepro.2020.121091

[32] G. Silversmit, D. Depla, H. Poelman, G. Marin, R. Gryse, Determination of the V2p XPS binding energies for different vanadium oxidation states ($V^{5+}$ to $V^{0+}$). J. Electron. Spectrosc. **135** (2-3), 167-175 (2004). DOI: https://doi.org/10.1016/j.elspec.2004.03.004

[33] E.L. Martin, K.E. Bentley, Spectrophotometric Investigation of Vanadium(II), Vanadium(III), and Vanadium(IV) in Various Media. Analytical Chemistry **34** (3), 354-358 (1962). DOI: https://doi.org/10.1021/ac60183a016

[34] W.H. Xiao, H.X. Zhao, N. Song, Leaching of Fe, V and Ti from pre-reduced vanadium-bearing titanomagnetite bulk concentrate with HCl and $H_2SO_4$. The Chinese Journal of Process Engineering **16** (1), 737-743 (2016). DOI: https://doi.org/10.12034/j.issn.1009-606X.216148

[35] C. Hugo, D. Endara, Recovery of Vanadium from Acid and Basic Leach Solutions of Spent Vanadium Pentoxide Catalysts **4** (1), 213-218 (2015). DOI: https://doi.org/10.17265/2328-2193/2015.04.006

[36] L. Wang, W. Sun, R. Liu, X. Gu, Flotation recovery of vanadium from low-grade stone coal. Trans. Nonferrous Met. Soc. China **24** (4), 1145-1151 (2014). DOI: https://doi.org/10.1016/S1003-6326(14)63173-3

[37] J. Larson, Thermochemistry of vanadium (5+) in aqueous solutions. J. Chem. Eng. Data. **40** (1), 1276-1280 (1996). DOI: https://doi.org/10.1021/je00022a030

[38] W. Zhang, T. Zhang, G. Lv, X. Cao, H. Zhu, Thermodynamic study on the V(V)-P(V)-$H_2O$ system in acidic leaching solution of vanadium-bearing converter slag. Sep. Purif. Technol. **218** (1), 164-172 (2019). DOI: https://doi.org/10.1016/j.seppur.2019.02.025